Journal of Molecular Modeling (2018) 24: 20
https://doi.org/10.1007/s00894-017-3567-6

ORIGINAL PAPER

CO oxidation on inverse Ce_6O_{12}/Cu(111) catalyst: role of copper–ceria interactions

Bing-Xing Yang [1,2,3] · Yong Luo [1,2,3,4] · Li-Ping Ye [1,2,3]

Received: 15 August 2017 / Accepted: 7 December 2017 / Published online: 20 December 2017

Abstract

The surface structures, O_2 adsorption, and CO oxidation reaction properties of Ce_6O_{12}/Cu(111) have been investigated using density functional theory including on-site Coulomb corrections (DFT + U). Results show that the supported ceria nanoparticles would gain electrons from the Cu(111) surface, and the Ce^{4+} are reduced to Ce^{3+}. In addition, the oxygens at the interface have been largely activated, resulting in much low formation energy of O vacancies. For the CO oxidation reaction, two possible pathways are investigated, CO reacts with the O_2 molecule adsorbed on Ce^{3+} and the lattice O at the interface, respectively. It has been found that CO reacting with the lattice O atom gives a lower reaction barrier than that of adsorbed O_2 on Ce^{3+}. These results are important for further understanding of the role of different active sites on the inverse CeO_x/Cu(111) surface structure.

Keywords DFT · CO oxidation · Copper-ceria interaction · Interface

Introduction

Inverse catalysts with oxide nanoparticles (NPs) supported on metal surfaces have attracted much attention for their high catalytic activity, even at relatively low temperatures, in many areas, such as water-gas shift (WGS) [1–3], CO oxidation [4, 5], and methanol synthesis from carbon dioxide [6, 7]. Interestingly, compared with the regular metal/oxide catalysts, the inverse ones sometimes show better activity [8, 9]. For example, compared with Cu/CeO_2, CeO_x/Cu(111) has higher catalytic activity for the WGS reaction [10, 11]. Furthermore, Au(111) and CeO_2 contribute no activity to the WGS reaction individually, but together they show remarkably activity [3]. The defects of ceria nanoparticles and the metal–oxide interface are considered the active sites.

✉ Li-Ping Ye
ylp_by@126.com

1 State Key Laboratory of Polyolefins and Catalysis, Shanghai 200062, People's Republic of China

2 Shanghai Key Laboratory of Catalysis Technology for Polyolefins, Shanghai 200062, People's Republic of China

3 Shanghai Research Institute of Chemical Industry CO., LTD, Shanghai 200062, People's Republic of China

4 Shanghai Institute of Technology, Shanghai 201418, People's Republic of China

Precious metals have been used for a long time for CO oxidation [12–14], but, due to the high price and low abundance of the latter, catalysts of non-noble metal are attracting increasing interest. Especially, CuO_x- and Cu-based catalysts are being recognised for their excellent activity [15–17]. CeO_2 has been used widely as a support in conventional metal/CeO_2 configurations for CO oxidation [18, 19]. And the inverse CeO_2/metal catalysts have also been studied experimentally in great detail [3, 9, 20]. The CeO_2–metal interaction generates active Ce^{3+} species in the oxide particle, which is related to the catalytic activity of the inverse system. This interaction was studied in situ by IRRAS and AP-XPS under WGS reaction (WGSR) conditions; the Cu–Ceria interaction caused the formation of Cu^{2+}/Cu^{+}(Cu^{0}) and Ce^{4+}/Ce^{3+} redox pairs [10]. For the CO oxidation reaction, the inverse CeO_x/Cu(111) system also exhibited high activity [4, 20, 21], which was similar to, or even better than, that of catalysts based on noble metals. The special properties of ceria NPs provide high O_2 dissociation activity, which is considered to be crucial for CO oxidation [21]. However, the identification of active sites on the surface structure of CeO_x/Cu(111) remains a challenging task, due to the complexity of the inverse system under real working conditions.

In this work, we performed systematic DFT calculations of the surface structural properties of the inverse Ce_6O_{12}/Cu(111) surface and its activity to oxidize CO. The active sites of the

ceria particle and the Cu–Ceria interface were studied in terms of oxygen activation and CO oxidation.

Computational details

All calculations were carried out using the Vienna ab initio simulation package (VASP) [22, 23], approached within the project-augmented wave (PAW) method [24, 25], and results were obtained using the MedeA® software environment [26]. The Perdew-Burke-Ernzerhof (PBE) [27] electron exchange-correlation functional based on the generalized gradient approximation (GGA) was employed. We treated the C 2 s, 2p, O 2 s, 2p, Cu 3d, 4 s, and Ce 4f, 5 s, 5p, 6d, 6 s as valence electrons. In order to correct for the description of the strong localization of the Ce 4f electrons, a Hubbard-like U term was used [28, 29], where U = 4.5 eV was applied to the Ce 4f states. This value was calculated self-consistently by Fabris et al. [30] for the cerium atoms in cerium oxides. The transition states in the reactions were determined by the climbing-image nudged elastic band (CI-NEB) method [31–36], and results obtained using MedeA® Transition State Search module. Vibrational analysis was also performed to insure the exact transition states were found. We then continued to calculate the electronic energies with zero-point energy (ZPE) correction [37]: $ZPE = \sum_I \left({}^1/_2\right) h\nu_I$, where h is the Planck constant, and ν_I the calculated real frequencies of the system.

For the Cu(111) surface slab, we used a 6 × 6 supercell with five Cu layers. To avoid the interaction between neighboring slabs, a vacuum layer of 15 Å between slabs was built. The Ce_6O_{12} NPs supported on Cu(111) (Ce_6O_{12}/Cu(111)) was shown in Fig. 1, which was described by previous literature reports [6, 9, 20]. For all structural optimizations, the bottom one layer was fixed, while the other slab atoms were allowed to move with a force threshold of 0.05 eV/Å. Spin polarization was considered in all the calculations. The energy cutoff of plane wave expansion was set to 400 eV and a Monkhorst-Pack [38] grid of 1 × 1 × 1 k-points mesh was used. For the gas-phase CO and O_2 energies, we build a 10 × 10 × 10 $Å^3$ lattice containing a CO/O_2 molecule.

The adsorption energy of CO and O_2 molecules is defined as:

$$E_{ads} = -\left(E_{Ce6O12/Cu+mol} - nE_{mol} - E_{Ce6O12/Cu}\right) \quad (1)$$

Where $E_{Ce6O12/Cu+mol}$ is the total energy of CO/O_2 adsorbed on the surface slab, E_{mol} and $E_{Ce6O12/Cu}$ are energies of CO/O_2 in the gas phase and the surface slab, respectively.

The formation energy of O vacancy (O_v) is defined as:

$$E_v = E_{Ce6O11/Cu} - E_{Ce6O12/Cu} + \frac{1}{2}E_{O2} \quad (2)$$

Where $E_{Ce6O11/Cu}$, $E_{Ce6O12/Cu}$ and E_{O2} are the energies of Ce_6O_{11}/Cu(111), bulk Ce_6O_{12}/Cu(111), and gas-phase O_2, respectively.

Results and discussion

Geometric and electronic properties

The Ce_6O_{12}/Cu(111) surface structure is illustrated in Fig. 1. The CeO_x cluster with triangle geometry has been found as the most stable structure previously, both theoretically and experimentally [8, 9]. Accordingly, such triangle structure was considered here for Ce_6O_{12}. The Ce_6O_{12} nanoparticles strongly interact with the support and the Cu(111) surface greatly stabilizes the oxide cluster. Both Ce and O ions are bound to Cu, which cause the structural change in the surface. One can see that the Cu(111) surface is rippled, as shown in Fig. 1b. Parts of the Cu atoms are pulled outward the surface and some are suppressed below, the distance between the vertical positions of the highest- and lowest-lying Cu atom in the top layer reached to 0.48 Å.

The Bader charge analyses (Table 1) showed that Cu(111) surface loses charge by as much as 1.8 e, and for all Ce atoms (Fig. 1a) of Ce_6O_{12}/Cu(111) are more positive than their counterparts in the Ce_6O_{12} cluster, indicating reduction of the nanoparticle support on Cu(111) surface. Compared with the Bader charge of Ce^{3+} (9.9 e) in bulk Ce_2O_3, these Ce ions should be considered the Ce^{3+}. A similar result was proposed

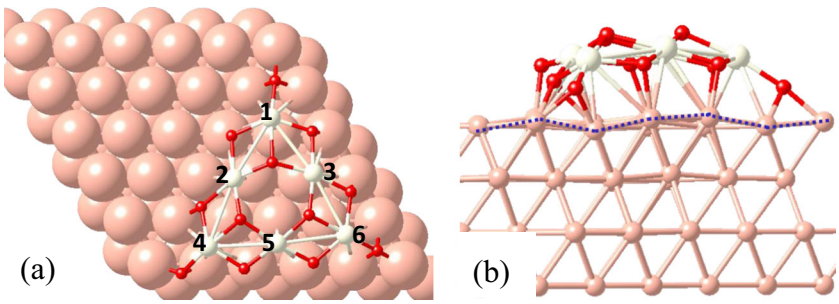

Fig. 1 **a** Top and **b** side views of the most stable Ce_6O_{12}/Cu(111) surface structures. Atoms: *Red* O, *pink* Cu, *white* Ce

Table 1 Calculated Bader charges (in e) of each Ce atom and all Cu atoms of Ce_6O_{12}/Cu(111), Ce_6O_{12} cluster, and Cu(111) surface

Number	Ce_6O_{12}/Cu(111)		Ce_6O_{12}	Cu(111)
	Ce	Cu	Ce	Cu
1	9.9341	1581.6	9.7101	1583.4
2	9.8726		9.7373	
3	9.8856		9.7206	
4	9.9438		9.7125	
5	9.9344		9.7214	
6	9.9201		9.7155	

by Graciani et al. [8], and they also proved that the strong interaction between the substrate and the supported nanoparticle overcame the loss of coordination and lowering of the Madelung electrostatic contribution in the ceria particles. Therefore, the special electronic and chemical properties of inverse Ce_6O_{12}/Cu(111) system provide good stability to support ceria and Ce^{3+} species.

O_2 adsorption on Ce^{3+} and O_v sites

As shown in Fig. 2a, for the molecular adsorption of O_2, significant relaxation occurred on the particles, and the O atoms moved into the interface, closer to the adsorbed O_2. In our previous work [39], we calculated the relaxation energy (E_{relax}) and bonding energy (E_{bond}), which are proved to be two important components of adsorption energy (E_{ads}). In this work, the E_{relax} is the energy gained from the structural relaxation in the presence of the adsorbed O_2, while the E_{bond} is the energy required to remove the O_2 with fixed structure of Ce_6O_{12}/Cu(111), and also the O_2 molecule is in the same geometry as it adsorbed. The calculated O_2 bonding energy was expressed as $E_{bond} = -\left(E_{Ce6O12/Cu+O2} - E^{fix}_{O2} - E^{fix}_{Ce6O12/Cu}\right)$.

According to Table 2, the calculated adsorption energy and bonding energy of O_2 at Ce^{3+} site is 2.09 eV and 0.71 eV, respectively. This clearly suggests that O_2 can chemisorb on Ce^{3+} of ceria nanoparticles, and the structural relaxation can also reduce the energy of the adsorption structure. The strong bonding strength and relaxation gives rise to the high adsorption energy of O_2. We then calculated the charge density difference, and also performed Bader charge analysis. As one can see from Fig. 2b, charge transfers from the substrate to the O atoms of adsorbed O_2 molecule, by as much as 1.08 e (Table 2), and the distance between them is 1.44 Å (Table 2), nearly the same as that reported by Li [40] for the peroxide (O_2^{2-}) species calculated on the defective CeO_2(111) surface. This indicates that the adsorbed O_2 at the interface of Ce_6O_{12}/Cu(111) is a peroxide (O_2^{2-}), and that the surface is reoxidized.

The calculated structures of Ce_6O_{12}/Cu(111) with one O_v and O_2 adsorption are shown in Fig. 2d,e, respectively. The corresponding energies are given in Table 2. The calculated O

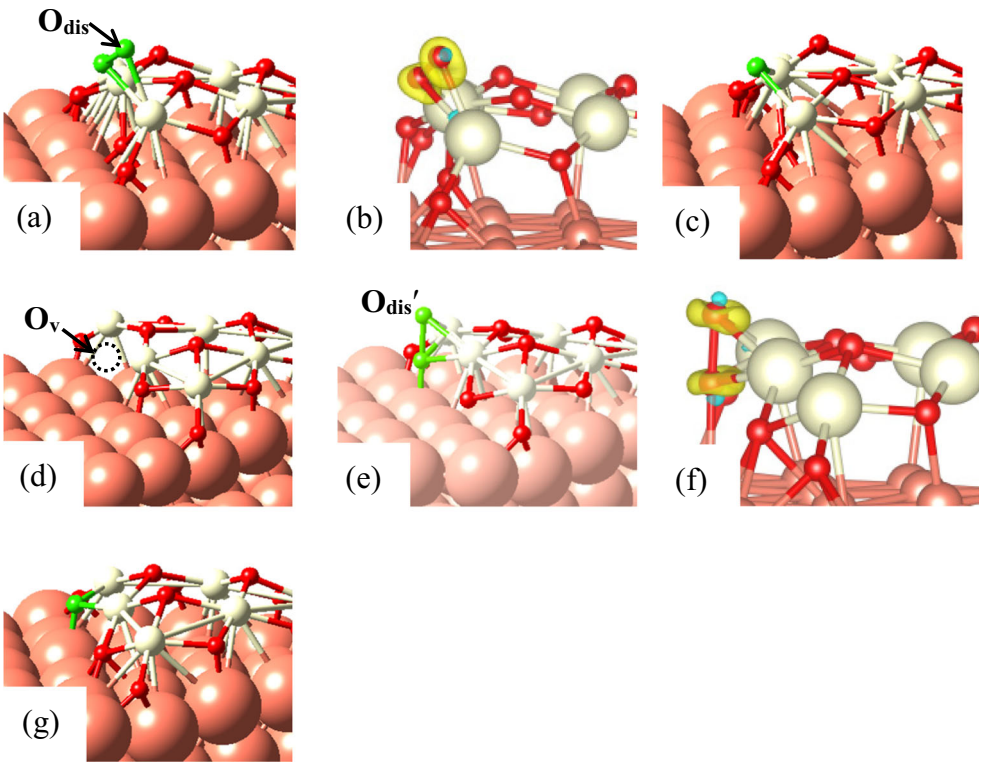

Fig. 2a–g Calculated structures of O_2 adsorption at the interface of Ce_6O_{12}/Cu(111). **a**, **c** Molecular and dissociative adsorptions, respectively; **d**, **e**, **g** Calculated structures of O vacancy and adsorbed O_2; **b**, **f** isosurfaces (0.02 e/ Å^3) of charge redistribution of **a** and **d**, respectively. The *yellow* and *blue* isosurfaces denote charge gain and loss, respectively. O atoms of O_2 are in *green*

Table 2 Calculated adsorption energies (E_{ads}, eV), bonding energies (E_{bond}, eV), reaction energies (ΔE, eV), O–O distances (Å), and Bader charge (e) of O_2 at Ce and O_v sites[a]

Sites	E_{ads}	E_{bond}	ΔE	O–O distance	Bader charge	Figure
Ce	2.09	0.71	5.61	1.44	1.08	2(a)
O_v	2.73	/	4.95	1.58	1.29	2(e)

[a] ZPE correction has been added to the E_{ads}, E_{bond}, ΔE

vacancy formation energy of the ceria nanoparticles is 1.74 eV, which is much lower than that in pure ceria [41], and O_2 adsorption occurs at the O_v with relatively high stability (2.73 eV). As shown in Fig. 2f, electrons transfer from the surface to the adsorbed O_2, by as much as 1.29 e (Table 2). The distance between O atoms of adsorbed O_2 is 1.58 Å, longer than that of O_2 adsorbed on Ce^{3+} (1.44 Å, Fig. 2a). These results show that the Cu(111) surface is able to promote the activity of the O atoms of ceria nanoparticles at the interface. Furthermore, O vacancy defects at the interface become active sites for O_2 adsorption and activation.

We then calculated the reaction energy for adsorbed O_2 dissociation as follows [2]: $\Delta E = 2*E(\text{O/surface}) - E(O_2/\text{surface}) - E(\text{surface})$. The dissociative O atoms at Ce^{3+} and O_v sites are represented as O_{dis} (Fig. 2a) and O_{dis}' (Fig. 2e). The calculated structures of O_2 dissociation at Ce^{3+} and O_v sites are shown in Fig. 2c,g, and the corresponding calculated ΔE is 5.61 eV and 4.95 eV (Table 2), respectively. One can see that the reactivity of O_2 dissociation on O_v is higher than that at the Ce^{3+} site. It is worth mentioning that we also tested the gas-phase CO reaction with the adsorbed O_2 at Ce^{3+} and O_v sites, and found that, during the static optimization, CO can combine with O_{dis}' to form CO_2 spontaneously, even if the length of the OC–O bond was set to 1.72 Å in the initial structure. On the contrary, no CO_2 formed at Ce^{3+} site though the gas-phase CO very closed to the O_{dis} (1.34 Å). This indicates that the adsorbed O_2 at O_v site is expected to be attacked directly by gas-phase CO molecules in the actual reaction conditions.

The reactions between gas-phase CO molecule and O_2^{2-} species on O_v and Ce^{3+} sites are shown in Fig. 3. As we can see, the energy barrier of CO reacting with O_{dis} is 1.17 eV, while it is only 0.13 eV for CO reacting with O_{dis}', in line with the results of reaction energy discussed above.

CO oxidation on interface

According to our calculations, CO molecules adsorb rather weakly on ceria nanoparticles. The calculated most stable CO adsorption structure is shown in Fig. 4a, as well as the coadsorption structure of CO and O_2 molecules (Fig. 4b). As we can see, CO adsorbs onto the hollow site of the Cu(111)

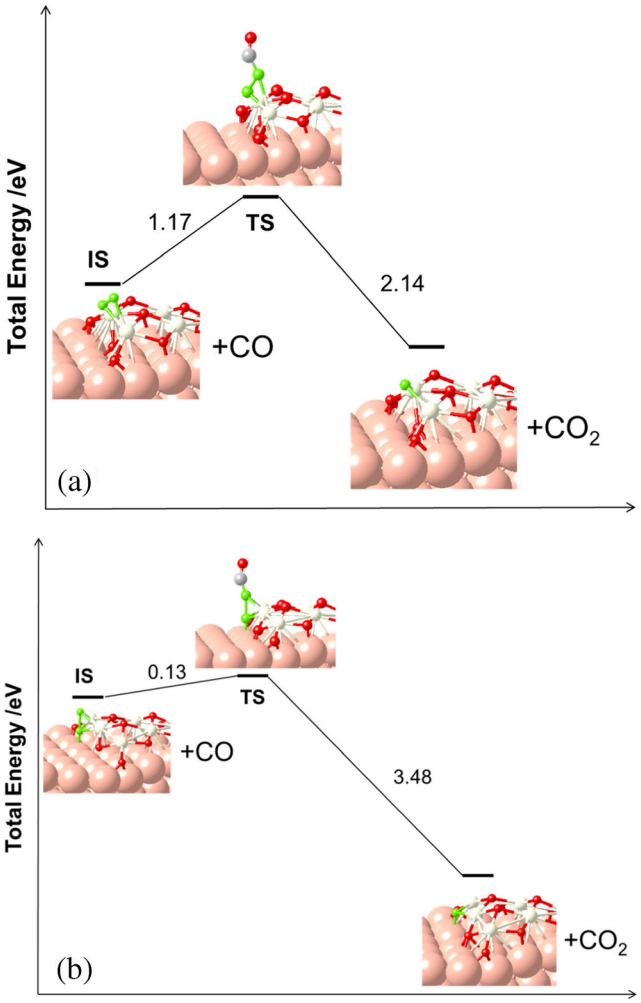

Fig. 3 Calculated energy profiles and structures of the important states of gas-phase CO reacting with **a** O_{dis} and **b** O_{dis}'

surface, and the adsorption energy is 1.13 eV. Both CO and O_2 are stably adsorbed on the interface.

We then studied two different routes of CO oxidation: (1) the reaction between adsorbed CO and O_2, and (2) CO oxidation with O atom of ceria nanoparticles at the interface. For the first reaction pathway, CO and O_2 can adsorb on the interface, and the CO molecule reacts with one O atom of the adsorbed O_2. Fig. 5a shows the transition state (TS) structure, the distance between the C atom of CO and the O atom of O_2 decreased from 3.64 Å in coadsorption state to 2.05 Å, and the barrier was estimated to be 1.27 eV. After the TS, CO_2 forms and desorbs, with a single O_{ad} left on the surface. As presented in Fig. 5(b), this O_{ad} can further react with another CO. The calculated adsorption energy for CO is 0.94 eV, and the reaction barrier is 0.91 eV. Therefore, it can be expected that this reaction path requires high activation energy, especially for the first step.

For the second pathway, the energy profile is depicted in Fig. 5c, from which we can see that the adsorbed CO molecule reacts directly with the O atom of ceria nanoparticles at the

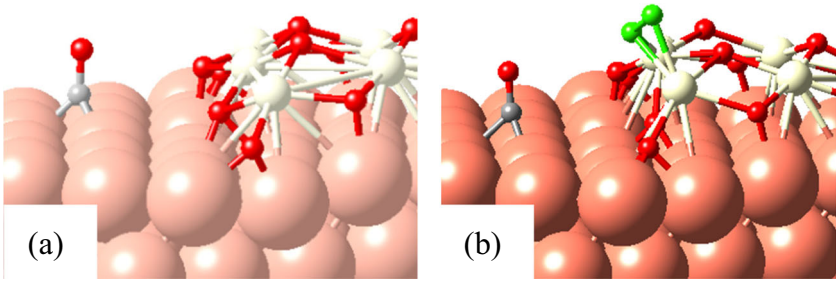

Fig. 4 Calculated structures of **a** CO adsorption, and **b** CO and O_2 coadsorption on Ce_6O_{12}/Cu(111)

interface by overcoming a barrier of 0.7 eV. This indicates that the strong interaction between ceria nanoparticles and the Cu(111) surface activated the O atoms of the particle much more than the adsorbed O_2 on it. With desorption of CO_2, an O vacancy formed at the interface (Fig. 2d). Then the O_v can be filled easily by adsorbed O_2. From our previous discussion, the adsorbed O_2 is activated by O_v. It is then attacked directly by gas-phase CO molecules, and the energy barrier is only 0.13 eV. With desorption of CO_2, a defect-free surface is left behind that can further oxidize CO.

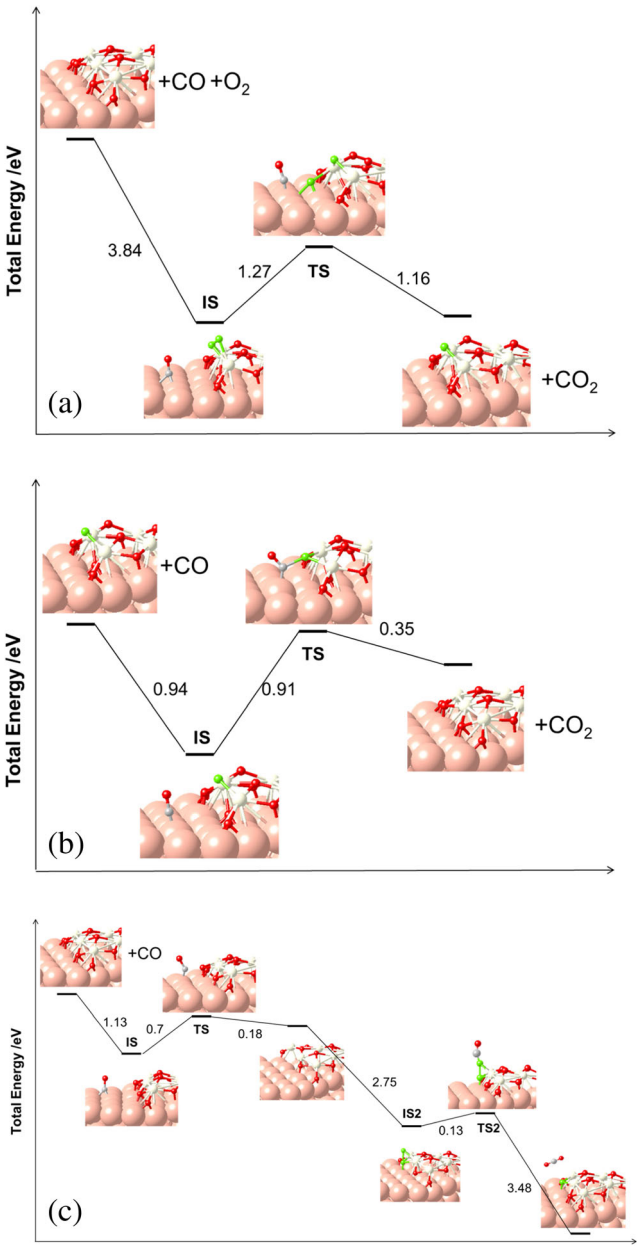

Fig. 5 Calculated energy profiles and structures of the important states of CO oxidation by **a** adsorbed O_2, **b** single O_{ad}, and **c** lattice O at the interface of Ce_6O_{12}/Cu(111)

Conclusions

Through DFT + U calculations, we have systematically studied the adsorption and reaction of CO and O_2 at the interface of the inverse Ce_6O_{12}/Cu(111) surface. According to our calculation results, the strong interaction between the substrate and the supported ceria nanoparticles causes the reduction of Ce ions, and activates the O_2 adsorbed on them. In particular, the O atoms of the supported particle at the interface proved to have higher reactivity with CO than that of adsorbed O_2 on Ce^{3+}, and the O_v defect can further active the O_2 adsorbed on it. The O_v defects at the interface of inverse CeO_x/Cu(111) surface are more likely to be the active sites for CO oxidation.

Acknowledgment This work was supported by Natural Science Foundation of Shanghai (15ZR1421500).

References

1. Senanayake SD, Stacchiola D, Evans J, Estrella M, Barrio L, Pérez M, Hrbek J, Rodriguez JA (2010) J Catal 271:392–400
2. Vidal AB, Liu P (2012) Phys Chem Chem Phys 14:16626–16632
3. Rodriguez JA, Ma S, Liu P, Hrbek J, Evans J, Pérez M (2007) Science 318:1757–1760
4. Ringleb F, Fujimori Y, Brown MA, Kaden WE, Calaza F, Kuhlenbeck H, Sterrer M, Freund HJ (2015) Catal Today 240: 206–213
5. Kim HY, Liu P (2015) J Phys Chem C 119:22985–22991
6. Graciani J, Mudiyanselage K, Xu F, Baber AE, Evans J, Senanayake SD, Stacchiola DJ, Liu P, Hrbek J, Sanz JF, Rodriguez JA (2014) Science 345:546–550
7. Senanayake SD, Ramírez PJ, Waluyo I, Kundu S, Mudiyanselage K, Liu ZY, Liu Z, Axnanda S, Stacchiola DJ, Evans J, Rodriguez JA (2016) J Phys Chem C 120:1778–1784

8. Graciani J, Vidal AB, Rodriguez JA, Sanz JF (2014) J Phys Chem C 118:26931–26938
9. Rodriguez JA, Graciani J, Evans J, Park JB, Yang F, Stacchiola DJ, Senanayake SD, Ma S, Pérez M, Liu P (2009) Angew Chemie Int Ed 48:8047–8050
10. Mudiyanselage K, Senanayake SD, Feria L, Kundu AE, Baber J, Graciani J, Vidal AB, Agnoli S, Evans J, Chang R, Axnanda S, Liu Z, Sanz JF, Liu P, Rodriguez JA, Stacchiola DJ (2013) Angew Chemie Int Ed 52:5101–5105
11. Rodriguez JA, Hrbek J (2010) Surf Sci 604:241–244
12. Suchorski Y, Wrobel R, Becker S, Weiss H (2008) J Phys Chem C 112:20012–20017
13. Xu J, While T, Li P, He C, Yu J, Yuan W, Han YF (2010) J Am Chem Soc 132:10398–10406
14. Cheng XL, Zhao YY, Li F, Liu YJ (2015) J Mol Model 21:230
15. Snytnikov PV, Popova MM, Men Y, Rebrov EV, Kolb G, Hessel V, Schouten JC, Sobyanin VA (2008) Appl Catal A 350:53–62
16. Rao KN, Bharali P, Thrimurthulu G, Reddy B (2010) Catal Commun 11:863
17. Huang TJ, Tsai DH (2003) Catal Lett 87:173–178
18. Zhang C, Michaelides A, Jenkins SJ (2011) Phys Chem Chem Phys 13:22–33
19. Rodriguez JA, Liu P, Hrbek J, Evans J, Pérez M (2009) Angew Chemie Int Ed 46:1329–1332
20. Yang F, Graciani J, Evans J, Liu P, Hrbek J, Sanz JF, Rodriguez JA (2011) J Am Chem Soc 133:3444–3451
21. Senanayake SD, Stacchiola D, Rodriguez JA (2013) Acc Chem Res 46:1702–1711
22. Kresse G, Furthmüller J (1996) Comput Mater Sci 6:15–50
23. Kresse G, Furthmüller J (1996) Phys Rev B 54:11169–11186
24. Kresse G, Joubert D (1999) Phys Rev B 59:1758–1775
25. Blöchl PE (1994) Phys Rev B 50:17953–17979
26. (2013) MedeA® is a registered trademark of Materials Design, Santa Fe, NM
27. Perdew JP, Burke K, Ernzerhof M (1996) Phys Rev Lett 77:3865–3868
28. Dudarev SL, Botton GA, Savrasov SY, Humphreys CJ, Sutton AP (1998) Phys Rev B 57:1505–1509
29. Anisimov VI, Aryasetiawan F, Lichtenstein AI (1997) J Phys Condens Matter 9:767–808
30. Fabris S, Gironcoli DS, Baroni S, Vicario G, Balducci G (2005) Phys Rev B 72:237102
31. Jonsson H, Mills G, Jacobsen KW (1998) Nudged elastic band method for finding minimum energy paths of transitions. World Scientific, Singapore
32. Henkelman G, Jónsson H (2000) J Chem Phys 113:9978–9985
33. Henkelman G, Uberuaga BP, Jónsson H (2000) J Chem Phys 113: 9901–9904
34. Sheppard D, Terrell R, Henkelman G (2008) J Chem Phys 128: 134106
35. Sheppard D, Henkelman G (2011) J Comput Chem 32:1769–1771
36. Sheppard D, Xiao P, Chemelewski W, Johnson DD, Henkelman G (2012) J Chem Phys 136:074103
37. Wynne-Jones WFK, Eyring H (1935) J Chem Phys 3:492–502
38. Monkhorst HJ, Pack JD (1976) Phys Rev B 13:5188
39. Yang BX, Ye LP, Gu HJ, Huang JH, Li HY, Luo Y (2015) J Mol Model 21:195
40. Li HY, Wang HF, Gong XQ, Guo YL, Guo Y, Lu GZ, Hu P (2009) Phys Rev B 79:193401
41. Mayernick AD, Janik MJ (2008) J Phys Chem C 112:14955–14964